Multi-scale material model for 3D composite using Micro CT Images geometry reconstruction

Yang Liu [a,*], Ilya Straumit [b], Dmytro Vasiukov [a], Stepan V. Lomov [b], Stéphane Panier [a]

[a] Polymers and Composites Technology & Mechanical Engineering Department, Ecole des Mines de Douai, France

[b] Department of Materials Engineering (MTM), KU Leuven, Belgium

*corresponding author: yang.liu@mines-douai.fr

Keywords: 3D composites, voxel model, micro CT, multi-scale modeling, damage mechanics

Abstract

Unit cell (UC) voxel models for 3D glass fiber/epoxy plain interlock composite were reconstructed based on the micro computed tomography (CT) data using ***VoxTex*** software. The predicted in-plane properties were compared with TexGen-generated model. Different elementary sub-UC models were also proposed to find out the optimum simulation scheme to reduce computational cost and maintain predictive accuracy. A progressive damage model was used to describe the nonlinear behavior for both matrix and yarns. The initiation and evolution of the meso-scale damage agreed well with the experimental observations.

1. Introduction

Compared to analytical (orientation averaging method [1–3]; inclusion method [4]) and semi-analytical (method of cells [5,6]) homogenization approaches, finite element (FE) method allows the use of a more complicated and realistic geometry for the long fibre reinforced composite (e.g. textiles and laminates) to determine the linear and nonlinear mechanical behavior, elasticity [7–9], elasto-plasticity [10] and failure mode analysis [11–14]. Geometric modelling strategy could be classified into two categories, i.e. the idealized and the realistic. A typical idealized model considers the yarns as aligned geometrical objects with constant cross-section and regular trajectories which may largely differ from the real geometry.

Naouar et al. have proposed a direct method to reconstruct the geometry suitable for any type of reinforcement from their micro CT images [15]. Image process techniques were repeated slice by slice to identify the different constituents. A skeletonisation scheme was implemented to find out the neutral axis of the yarn which would further be used to determine the local material orientation. Authors have employed the front algorithm to discretize the geometry with tetrahedral elements for FE usage. The proposed real geometry presented a compaction simulation result closer to the experiment one than the purely idealized model. Nevertheless, the tetrahedron meshing scheme inevitably increases the time cost in both pre- and post- process since adapting the curved surface of yarn will result in a huge amount of generated elements.

New reconstruction scheme, used in this work is able to better reflect the real architecture and at the same time the meshing scheme permits high computational efficiency. Straumit et al. developed a software package named ***VoxTex*** which enable an automatic generation of "voxelized" model from the micro CT

Excerpt from ISBN 978-3-00-053387-7

image [16]. A 3D virtual volume model is initially prepared by stacking the images slice by slice. Then the user defined voxel size and integration window need to be assigned to form a discretized volume with the specified mesh density. After that, by processing the 3x3 matrix of the structural tensor for each voxel, three eigenvalue and eigenvector pairs can be determined. The eigenvector which corresponds to the minimum eigenvalue is taken as the principal direction of the calculated voxel. Some basic segmentation algorithm, like thresholding method and the K-means clustering method have been integrated for the separation of constituents. A more sophisticated scheme which allows segmentation between warp and weft yarns will be discussed in Section 3.

Experimental work centered on 3D glass fiber plain interlock composite will be introduced in next section. The generation of real and idealized geometric models would be detailed subsequently. FE calculation schemes to simulate both linear and nonlinear behavior for different models are illustrated followed by a comparative study and results discussion. Conclusions and perspectives are made in the last section.

2. Experimental preparation

The infusion technique is employed for impregnating the 3D glass-fiber plain interlock preforms. Epolam 5015 epoxy and 5015 hardener (Axson Technology®) are mixed with mass ratio 100:30. Resin properties are shown in Table 1. The injection of the resin is driven by -0.9 bar pressure. The impregnated tissue is cured in an autoclave at 50 °C for 2 hours until complete polymerization.

Young's Modulus	3.0 GPa
Tensile strength	80 MPa
Elongation at break	6%
Cured density	1.10 g/cm^3
Viscosity at 25°C	0.21Pa.s

Table 1. Properties of Epolam 5015 resin

The determination of total fiber volume fraction V_f for a pure glass fiber reinforced composite can be done with the burn-off test. Hence 5 (20x20 mm) samples cutting from 2 different interlock plates were burnt during 4 hours at 550°C inside the furnace. The mean V_f for the 3D plain interlock composite locates at 40.3% with standard deviation 0.86%. Optical microscope observation was conducted to assess the local fiber volume fraction of the yarn $V_{f,\mathrm{Y}}$ in combination with the image process techniques.

The microscopic observation in fiber scale was conducted by X-ray CT scanning system (160 kV voltage and 4.06μm/pixel resolution). Fig. 1(a) shows a typical 2D morphology of the internal architecture of 3D plain interlock. The green box roughly profiles the boundary of a UC along thickness and weft yarn direction. Fig. 1(b) presents the realistic yarn geometry reconstructed by Avizo® with the matrix hidden.

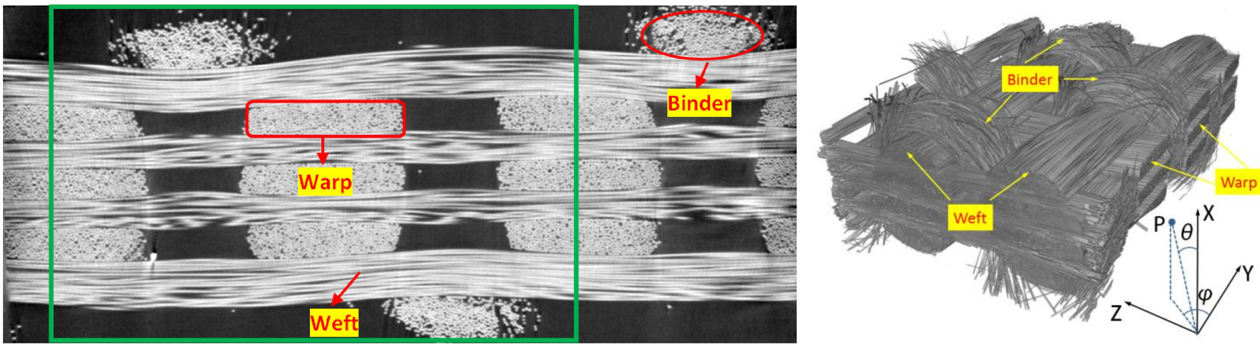

(a) (b)

Fig. 1. (a) 2D and (b) 3D real morphology of the scanned 3D interlock composite sample

Excerpt from ISBN 978-3-00-053387-7

Standard specimen oriented along weft, warp and 45° bias yarn direction were cut out from the composite plates respectively. The gradually increased loading/unloading tests were carried out on Instron 1185 test machine with a cross-head speed of 3 mm/min. A CCD was used to capture the image of the deformed specimen surface every 0.25 second. Digital image correlation method was implemented to measure the strain fields with commercial software Vic-2D®. The experimental in-plane mechanical properties will be compared with the prediction results of FE models.

3. Generation of FE models

3.1 Real model

A region of interest (ROI) with 2.76mm length, 2.76mm width and 1.98mm thickness, which can be approximately considered as a unit cell, is cut out and discretized into voxel model with integration radius for calculation of the structure tensor of 8 pixels. When two-variable (degree of anisotropy and average grey value for this case) clustering segmentation scheme is imposed, the ROI is separated into only two parts, i.e. yarns and matrix, as shown in Fig. 2 - Fig. 4.

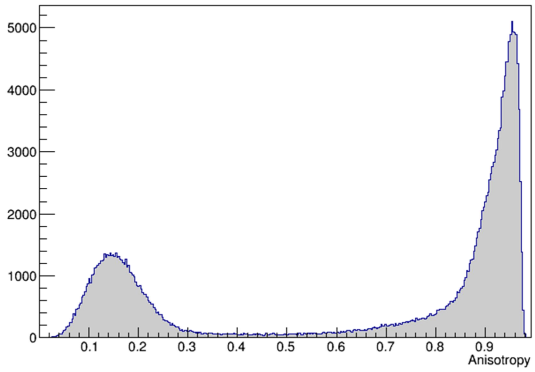

Fig. 2. The histogram of degree of anisotropy in the voxel model

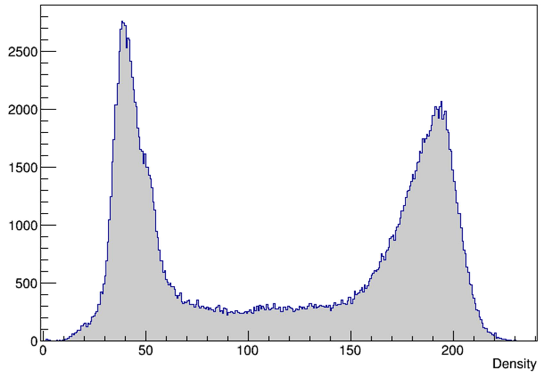

Fig. 3. The histogram of grey value in the voxel model

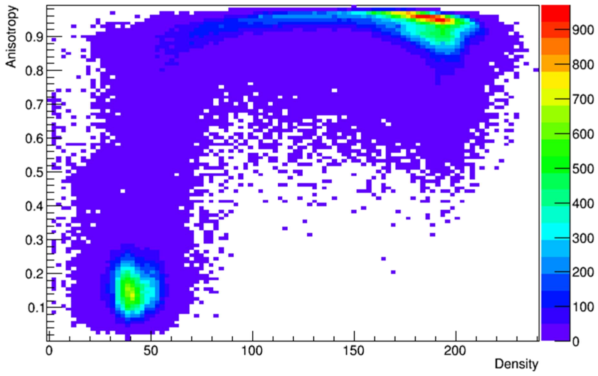

Fig. 4. Histogram of the degree of anisotropy versus average grey value computed from the voxel model.

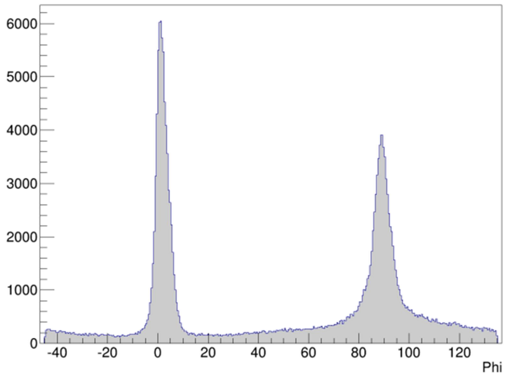

Fig. 5. Histogram of ϕ in spherical coordinate system, derived from the micro-CT image of the material

Therefore, to better reflect the real architecture, another smart "supervised learning" segmentation scheme was programmed and integrated into *VoxTex* for further subdivision of the yarn. A training set, which sufficiently grasps the distinct features for each constituent, was created so that a to-be-segmented sub-volume could be "supervised". The azimuthal angle ϕ, on the YZ projection plane, refer to Fig. 1(b), plays a critical role to separate the warp/binder ($\phi=90^{\circ}$) from weft ($\phi=0^{\circ}$) as shown in Fig. 5. A well segmented UC model with 212,658 C3D8 elements is shown in Fig. 6. Kinematic uniform boundary conditions (KUBC) are imposed. 1/2 and 1/4 UC models, as shown in Fig. 7 and Fig. 8, are also generated by partitioning the scanning image from different positions.

Excerpt from ISBN 978-3-00-053387-7

3.2 Idealized model

An idealized UC model with 3.38 mm length, 2.89 mm width and 1.98 mm thickness for the same composite was generated by TexGen, see to Fig. 9. The constant cross-sectional yarns were organized in a column aligned way and the non-waviness assumption was applied for warp and weft yarns to simplify the geometry. A voxel model with 302,400 C3D8 elements was exported for FE usage. The mesh density was as same as the real model. For each yarn element the local orientation was derived inherently according to centerline of the yarn. Periodic BCs is imposed onto the UC model due to periodically repetitive geometry of the textile.

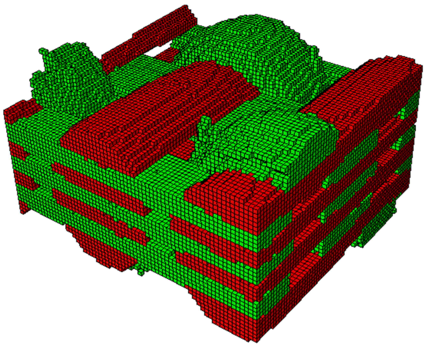

Fig. 6. The voxel model of the unit cell generated by *VoxTex* (with the matrix hidden)

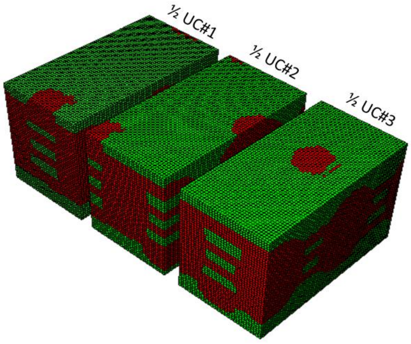

Fig. 7. 1/2 unit cell models for FE calculation usage

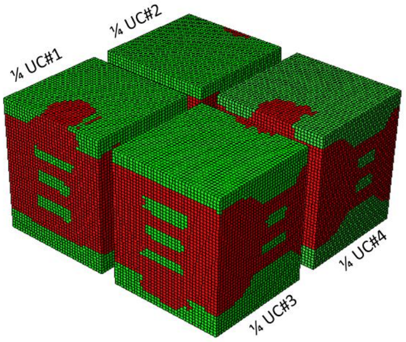

Fig. 8. 1/4 unit cell models for FE calculation usage

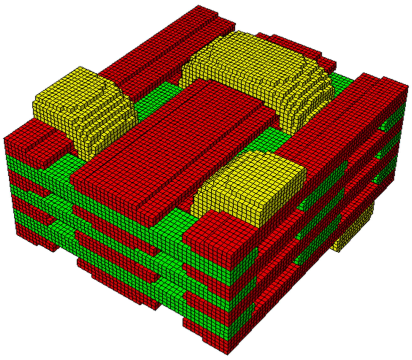

Fig. 9. The voxel model of the unit cell generated by *TexGen* (with the matrix hidden)

3.3 Constituent properties

The global fiber volume fraction of the model V_f, the local fiber volume fraction of yarn $V_{f,Y}$ and the total volume fraction of yarn V_Y are listed in Table 2 for each yarn in both real and idealized models. On the basis of the naked-eye and the optical microscope observations, both the weft and the warp yarns can be considered as constant cross-sectional and sufficiently infused so that the image process technique can be used to measure the $V_{f,Y}$, while for the binder the above measurement was not applicable anymore due to the changeable cross-section and damaged geometry. Inverse method was employed to determine the average $V_{f,Y}$ of binder yarn by the known parameters including total V_f, V_Y for each yarn (estimated form FE model) and $V_{f,Y}$ for the warp (just for idealized case because in the present real model, binder yarns and the warp yarns cannot yet be separated from each other) and weft yarn. In 1/2 and 1/4 UC models the $V_{f,Y}$ of each yarn keeps the same as that of the real UC model.

Chamis' model [17] is then used to estimate the effective properties of the impregnated yarn by knowing the basic mechanical properties of isotropic matrix (Young's modulus 3.0 GPa, Poisson ratio 0.3) and isotropic E-Glass fiber (Young's modulus 72.0 GPa, Poisson ratio 0.3) together with the of local fiber content $V_{f,Y}$.

Excerpt from ISBN 978-3-00-053387-7

		Idealized UC model		Real UC model	
Weft yarn		V_Y=29.0%	$V_{f,Y}$=75.7%	V_Y=27.4%	$V_{f,Y}$=75.7%
Warp yarn	Binder	V_Y=12.2%	$V_{f,Y}$=56.7%	V_Y=28.0%	$V_{f,Y}$=69.9%
	Straight	V_Y=15.2%	$V_{f,Y}$=75.7%		
Total V_Y		56.3%		55.4%	
Total V_f (40.3% exp.)		40.3%		40.3%	

Table 2. The fiber/yarn volume fraction for both real and idealized UC models.

4. Progressive damage modelling

The following is a brief introduction of the damage model for the impregnated yarns. The failure initiation criterion is based on the Hashin's 3D as shown in [18]. Damage effect tensor is similar to one presented in [19]. The exponential damage evolution laws have been used,

$$d_i = 1 - \frac{1}{f_i} e^{(1-f_i)\beta} \qquad (i = f_1, d_{m1}, d_{m2}) \tag{1}$$

where f_i are scaling function according to initiation criterion for i damage mechanisms and β is quantity related to critical energy release rate and element characteristic length according to cracks smeared theory. Damage model was derived based on the energy equivalent principle. In case of resin material, the isotropic damage model was applied. The constitutive model of the polymer resin comprises elastic and damage behavior. The pressure dependent damage initiation function has been used in the following form as shown in Eq. 2. The resin micro-cracking has isotropic damage effect only.

$$\begin{gathered} f_{init} = \sqrt{C_1 J_{2D}^{\varepsilon}} + C_2 I_1^{\varepsilon} \le 1 \\ where\ C_1 = 1/(\varepsilon_T \varepsilon_C),\ C2 = 3(\varepsilon_C - \varepsilon_T)/(\varepsilon_T \varepsilon_C),\ J_{2D}^{\varepsilon} = (\frac{1}{3} I_1^{\varepsilon})^2 - 3 I_2^{\varepsilon}, \\ I_1^{\varepsilon} = (\varepsilon_{11} + \varepsilon_{22} + \varepsilon_{33}),\ I_2^{\varepsilon} = \varepsilon_{12}^2 + \varepsilon_{23}^2 + \varepsilon_{31}^2 - \varepsilon_{11}\varepsilon_{22} - \varepsilon_{22}\varepsilon_{33} - \varepsilon_{33}\varepsilon_{11} \end{gathered} \tag{2}$$

Both isotropic and anisotropic damage models, for matrix and yarns respectively, were implemented with ABAQUS/UMAT. Viscous regularization was applied to facilitate the convergence.

5. Homogenization scheme

6 group of independent displacement loading cases were applied onto a FE model for an elastic behavior analysis, hence the volume averaging scheme was implemented to homogenize the effective stress component $\bar{\sigma}_{ij}$

$$\overline{\sigma}_{ij} = \iiint_V \sigma_{ij}\, dV = \sum_{ne}^{NE} \iiint_{V^e} \sigma_{ij}\, dV^e = \sum_{ne=1}^{NE} \sum_{ni=1}^{NI} \sigma_{ij}(I) \cdot W(I) \cdot J(I) \tag{3}$$

where NE is the total number of element in the model, NI is the number of Gaussian integration point (IP) in an element, $\bar{\bar{\sigma}}_{ij}(I)$ is stress component value on a certain IP, W(I) and J(I) denotes respectively the weight value and the Jacobian value corresponding to that IP. A Python post-process code is written to calculate the averaged stress components and the effective elastic properties.

6. Results analysis

6.1 In-plane effective properties

Excerpt from ISBN 978-3-00-053387-7

The homogenized effective elastic moduli along warp, weft and 45° directions, the relative error with the experimental value are listed in Table 3 and drawn in Fig.11. Almost all the effective moduli predicted by the proposed numerical models lay within the experimental error range. UC model generated by *VoxTex* based on real geometry presents high accuracy to predict the all in-plane effective moduli while idealized model overestimated the E_{weft} significantly with an error of 8.71%. The prediction accuracy of 1/2 and 1/4 UC models are close to each other and the results of the former vary less than the latter. Therefore to reduce computational cost and maintain an acceptable accuracy 1/2 UC models are more recommended.

	Experimental	Idealized UC	Real UC	½ real UC	¼ real UC
E_{warp} (GPa)	15.8	15.8	16.0	16.3	16.3
	±4.4%	+0.4%	+1.7%	+3.1%	+3.1%
E_{weft} (GPa)	19.3	21.0	19.7	20.0	19.7
	±8.3%	+8.7%	+2.1%	+3.6%	+2.2%
$E_{45°}$ (GPa)	11.0	10.3	10.8	10.9	10.7
	±4.7%	-2. 6%	-1.6%	-0.8%	-2.3%

Table 3. The predicted in-plane effective properties of real and idealized models

6.2 Damage behavior analysis

An example of the modelled behavior in the warp direction is shown in Fig. 11. There are four main steps have been distinguished: initial elastic behavior, in general very short one which is followed by early initiation of transverse damage in bender yarns; then microcracking in resin start developing and the last step is fiber failure in the warp yarns, which for this loading case is final mechanism.

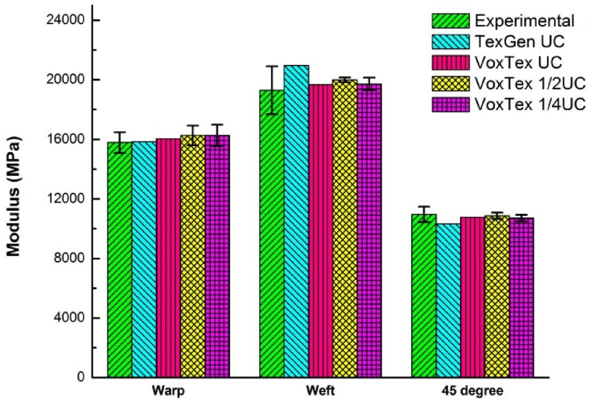

Fig. 10. In-plane properties predicted by different real and idealized models

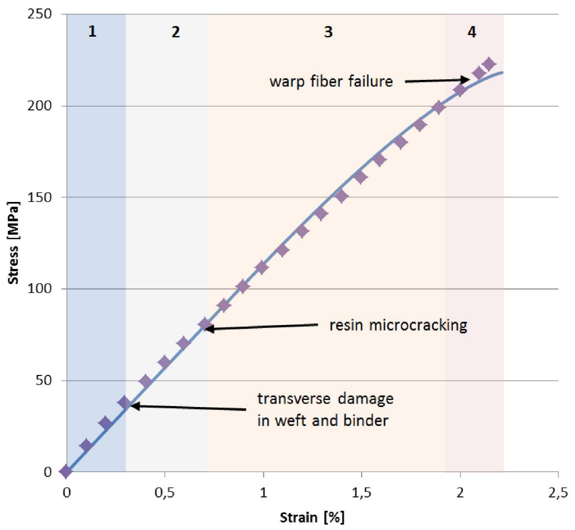

Fig. 11. Experimental and simulation nonlinear behavior (dot is experiment, line is modelling)

In Figs 12, 13 the calculated damage modes are shown for different yarns in weft and warp direction, the latter one is combined with binder yarns. Since the current model does not contain predefined interfaces the term debonding is included into the transverse damage of the yarns. The highest level of material degradation is observed near zones where different yarns are close to each other (weft/warp, binder/weft and binder/warp).

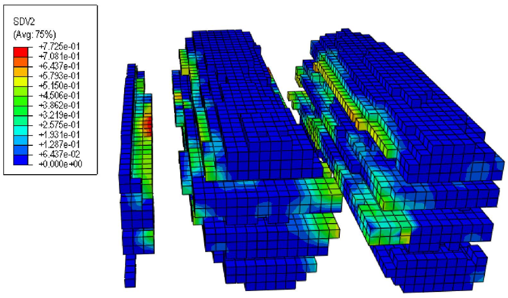

Fig. 12. Damage in the weft yarns and debonding localization

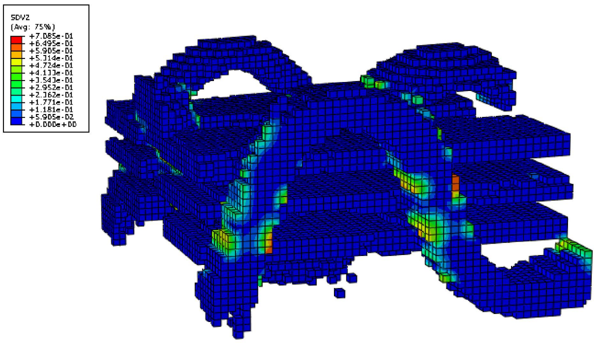

Fig. 13. Initiation of the transverse damage in binder yarn

7. Conclusions

Systematic experiments have been conducted, from the composite plate preparation (infusion) to meso-mechanical parameters determination (burn-off test, optical microscope observations and micro CT scanning) until to the macro-mechanical behavior tests.

Real UC geometry was reconstructed from the micro CT scanning images by a powerful pre-processor *VoxTex* and presented as a voxel model. 1/2 and 1/4 UC models were also generated to find an optimum simulation scheme to reduce the computational cost and maintain an acceptable accuracy. An idealized UC model with geometric parameters derived from the micro CT images has been generated for comparison. Properties predicted from real geometry show excellent agreement with those of experiments while significant error existed for E_{weft} prediction with idealized model. Computational costs could be reduced significantly by considering 1/2 UC geometry which provide desirable results.

At last, the results from loading/unloading tests were compared with nonlinear multi-scale simulations. The initiation and evolution of the meso-scale damage mechanisms have been analyzed and discussed. Qualitative results of the numerical simulation are in good agreement with experimental observations. Based on the real UC model, the predictive errors for in-plane elastic properties are below 2.1% while for the overall macroscopic nonlinear response the error does not exceed 10 % compared to the experiments.

Acknowledgement

One of the authors (Yang LIU) wishes to acknowledge sincerely the financial support of the China Scholarship Council such that this research can be undertaken. S.V. Lomov is a Toray professor (Toray Chair for Composite Materials in KU Leuven).

References

[1] El Hage C, Younès R, Aboura Z, Benzeggagh ML, Zoaeter M. Analytical and numerical modeling of mechanical properties of orthogonal 3D CFRP. Compos Sci Technol 2009;69:111–6.

[2] Nehme S, Hallal A, Fardoun F, Younes R, Hagege B, Aboura Z, et al. Numeric-alanalytical methods to evaluate the mechanical behavior of interlock composites. J Compos Mater 2011;45:1699–716.

[3] Hallal A, Younes R, Fardoun F, Nehme S. Improved analytical model to predict the effective elastic properties of 2.5D interlock woven fabrics composite. Compos Struct 2012;94:3009–28.

[4] Perie G, Lomov S, Verpoest I. Meso-scale modelling and homogenisation of interlock reinforced composite. 2nd World Conf. 3D Fabr., Greenville, South Carolina, USA: 2009.

[5] Bigaud D, Hamelin P. Mechanical properties prediction of textile-reinforced composite materials using a multiscale energetic approach. Compos Struct 1997;38:361–71. doi:10.1016/S0263-8223(97)00071-8.

[6] Prodromou AG, Lomov S V., Verpoest I. The method of cells and the mechanical properties of textile composites. Compos Struct 2011;93:1290–9.

[7] Wang XF, Wang XW, Zhou GM, Zhou CW. Multi-scale Analyses of 3D Woven Composite Based On Periodicity Boundary Conditions. J Compos Mater 2007;41:1773–88. doi:10.1177/0021998306069891.

[8] Qing H, Mishnaevsky Jr. L. 3D constitutive model of anisotropic damage for unidirectional ply based on physical failure mechanisms. Comput Mater Sci 2010;50:479–86.

[9] Lapeyronnie P, Le Grognec P, Binétruy C, Boussu F. Homogenization of the elastic behavior of a layer-to-layer angle-interlock composite. Compos Struct 2011:2795–807.

[10] Chen JF, Morozov EV, Shankar K. A combined elastoplastic damage model for progressive failure analysis of composite materials and structures. Compos Struct 2012;94:3478–89. doi:10.1016/j.compstruct.2012.04.021.

[11] Visrolia A, Meo M. Multiscale damage modelling of 3D weave composite by asymptotic homogenisation. Compos Struct 2013;95:105–13. doi:10.1016/j.compstruct.2012.07.018.

[12] Lu Z, Zhou Y, Yang Z, Liu Q. Multi-scale finite element analysis of 2.5D woven fabric composites under on-axis and off-axis tension. Comput Mater Sci 2013:485–94.

[13] Green SD, Matveev MY, Long AC, Ivanov D, Hallett SR. Mechanical modelling of 3D woven composites considering realistic unit cell geometry. Compos Struct 2014;118:284–93.

[14] Zhang C, Li N, Wang W, Binienda WK, Fang H. Progressive damage simulation of triaxially braided composite using a 3D meso-scale finite element model. Compos Struct 2015;125:104–16.

[15] Naouar N, Vidal-Sallé E, Schneider J, Marie E, Boisse P. Meso-scale FE analyses of textile composite reinforcement deformation based on X-ray computed tomography. Compos Struct 2014:156–76.

[16] Straumit I, Lomov S V., Wevers M. Quantification of the internal structure and automatic generation of voxel models of textile composites from X-ray computed tomography data. Compos Part A Appl Sci Manuf 2014;69:150–8. doi:10.1016/j.compositesa.2014.11.016.

[17] Chamis C. Mechanics of composite materials: Past, present and future. NASA Tech Memo 1984:1–40.

[18] Kress G. Examination of Hashin's failure criteria for the second world-wide failure exercise. J Comp Mats 2012;19-20:2536–61.

[19] Vasiukov D, Panier S, Hachemi A. Non-linear material modeling of fiber-reinforced polymers based on coupled viscoelasticity–viscoplasticity with anisotropic continuous damage mechanics. Compos Struct 2015;132:527–35. doi:10.1016/j.compstruct.2015.05.027.